Water-based enhancement of the resonant photoacoustic signal from methane–air samples excited at 3.3 μm

N. Barreiro · A. Peuriot · G. Santiago · V. Slezak

Abstract Photoacoustic spectroscopy is widely applied for trace-gas detection because of its sensitivity and low detection limit. In a previous work, where we studied the potential application to methane monitoring under a resonant excitation at 3.3 μm, we showed that the signal from methane–nitrogen mixtures decreases with the addition of oxygen. This effect is due to an energy exchange between the ν_4 asymmetric stretching mode of methane and the first metastable level of oxygen. This process makes oxygen accumulate energy, thus hindering the generation of the photoacoustic signal. In this work, we study the possible addition of water, as a good collisional partner of oxygen, in order to obtain a greater sensitivity. We develop a model based on rate equations and find good agreement between theory and measurements. The experiment is carried out with a novel cell of rectangular cross section and a Q factor of 165 ± 1. We find that 0.7 % water content is large enough to obtain a signal as high as in the methane–nitrogen case at atmospheric pressure.

N. Barreiro (✉) · A. Peuriot · V. Slezak
CEILAP-UNIDEF (CITEDEF-CONICET), Juan Bautista de La Salle 4397, 1603 Villa Martelli, Argentina
e-mail: nbarreiro@citedef.gob.ar

A. Peuriot
e-mail: apeuriot@citedef.gob.ar

V. Slezak
e-mail: vslezak@citedef.gob.ar

G. Santiago
GLOMAE, Facultad de Ingeniería, Universidad de Buenos Aires, Paseo Colón 850, 1063 Buenos Aires, Argentina
e-mail: gsantia@fi.uba.ar

1 Introduction

Methane is one of the main greenhouse effect gases. Its concentration has been increasing at a high rate due to multiple sources; in fact, it trebled during the last 150 years reaching a level of around 1.7 ppmV. Therefore, the availability of sensitive and selective methods for monitoring of methane in the atmosphere and its emission sources is important. The photoacoustic (PA) technique is a well-known method for trace-gas detection because of its wide dynamic range, selectivity and sensitivity [1, 2]. Thus, its application to methane detection is worth studying [3, 4].

In a previous paper [5], we showed that the PA signal from methane–dry air mixtures, excited by an optical parametric oscillator (OPO) at around 3.3 μm, is smaller than those found in methane–nitrogen mixtures because of oxygen's slow relaxation rate. The close-matching vibrational levels (methane's ν_b-bending mode and oxygen's ν-mode) exchange energy through vibration–vibration (V–V) processes in around 10^{-8} s for mixtures in air at atmospheric pressure [4]. In this way, most of the energy absorbed by methane is stored in the metastable ν level of oxygen instead of being totally transferred to kinetic energy. This phenomenon raises the PA detection limit and, sometimes, the system output may deviate from linearity [4]. That is why in these cases it is useful to look for a good collisional partner for oxygen to speed up energy release to the surroundings through vibration–translation (V–T) processes. It has been shown [4] that adding helium to the gas mixture increases the signal significantly, but a helium fraction as high as 10 % is needed to attain the amplitude obtained from methane in pure nitrogen because its energy exchange rate is not fast enough. Moreover, helium is not a natural component of the atmosphere, so adding it to a flow at atmospheric pressure introduces an undesirable difficulty to the measuring system. Therefore, finding a gas with faster V–T transfer rates

is worth pursuing. Huestis [6] showed that water presents a fast energy exchange rate with oxygen and, most important, it is a natural constituent of the atmosphere. In this sense, some authors [4, 7] have shown that water is an appropriate candidate as a collisional partner of oxygen to improve methane monitoring by the PA technique in the mid-infrared region. Moreover, water also increases the PA signal from CO_2 samples in N_2 excited at 1431 nm [8].

It is worth mentioning that there are several works that refer to the PA signal decrease due to the vibrational energy stored in metastable states of diatomic molecules after excitation of certain molecules. As an example, we can mention the effect of N_2 on IR-excited CO_2 [9–11] or HCN [12] and the subsequent signal increase after adding other gases (H_2O or noble gases).

In this work, we experimentally show that adding water to a methane–air mixture (excited at 3.3 μm) increases the PA signal. In addition, we show that the results are fairly described by means of a numerical kinetic model. The measurements on methane samples in different buffer gases are performed in a novel, simple acoustic cavity that allows us to obtain good sensitivity and low detection limit.

2 Model for the PA signal generation

The resonant PA technique is based on the excitation of a gas by laser radiation modulated at an eigenfrequency of an acoustic cavity. The laser wavelength is suitably chosen to excite the target gas species. The molecules transfer the absorbed energy through collisions to the surrounding buffer gas. This energy release produces an acoustic wave, readily detected with a microphone. A small V–T relaxation time (compared to the modulation period) ensures that little energy is lost through collisions between the molecules and the cell's wall.

In a previous work [5], we presented a simple kinetic model to calculate the released heat in methane–nitrogen–oxygen. Using an OPO tuned at 3.3 μm, we found an adequate agreement between the model and the experimental results. We concluded that it is necessary to add a new component to the system to increase the signal from methane–air samples. In this work, we choose water owing to its relaxation properties and because it is a natural component of the atmosphere. In the next sections, we revisit our kinetic model, this time introducing one excited vibrational level of water to analyze if the PA signal increase is predictable.

2.1 Hypothesis of the model

The vibrational modes of methane can be divided into two groups: the IR-active one, consisting of two modes conventionally denominated ν_3 and ν_4, and the IR-inactive one, involving the ν_1 and ν_2 modes. The wavenumbers of the ν_2

and ν_4 bending modes (ν_b) are 1533 and 1311 cm^{-1}, respectively. On the other hand, the ν_1 and ν_3 stretching modes (ν_S) at 2917 and 3019 cm^{-1}, respectively, have wavenumber values approximately twice those of the bending modes. These particular characteristics lead to a distribution of the vibrational levels in polyads. For example, the first polyad, the dyad, is formed by two states ν_2 and ν_4. The second polyad, the pentad, is formed by $2\nu_2$, $2\nu_4$, $\nu_2 + \nu_4$, ν_1 and ν_3. The proximity of the states inside a polyad enables a very fast energy exchange (approx. 10^{-9} s at atmospheric pressure), called intermode transfer. Another important characteristic of methane is that energy transfer between polyads happens essentially through the lowest vibrational quantum (ν_4).

Oxygen is a molecule with only one non-IR active vibrational mode (ν), whose value closely matches methane's bending vibrational modes. For this reason, there is a strong energy exchange between the dyad and ν. Once the oxygen is excited, the energy is stored in it because of its large relaxation time; this leads to a smaller PA signal compared to the CH_4–N_2 case.

The water molecule has three vibrational modes ν_1, ν_2 and ν_3 which correspond to symmetric stretching at 3657 cm^{-1}, bending at 1595 cm^{-1} and asymmetric stretching at 3756 cm^{-1}, respectively. As the three modes are IR active, this molecule presents a wide absorption spectrum. Some authors [4, 6, 13] have shown that there is a strong interaction between water and oxygen that speeds up V–V and V–T exchanges. In this way, the energy stored in oxygen can be rapidly released into kinetic energy through collisions with water.

To develop a kinetic model that allows predicting the PA signal, taking into account the energy levels and their interactions, we assume some hypotheses necessary to simplify the problem:

1. As stated formerly, the methane levels are distributed in polyads. We consider only the exchange between the ground state and the first two polyads.
2. The redistribution of energy inside a polyad is almost instantaneous. In this way, we can represent the pentad energy levels as ν_S (symmetric and asymmetric stretching modes) and $2\nu_b$ (harmonic and combination of the bending modes) and the dyad as ν_b.
3. The energy exchange between polyads and with the other gases happens only via the lowest energy quantum ($h\nu_4$).
4. Second-order processes are neglected. With this hypothesis, together with the third one, we can ignore the doubly excited levels of oxygen and water.
5. The V–T relaxation processes from the excited water molecules are very fast. Therefore, the PA signals from water and methane can be considered separately and linearly combined.
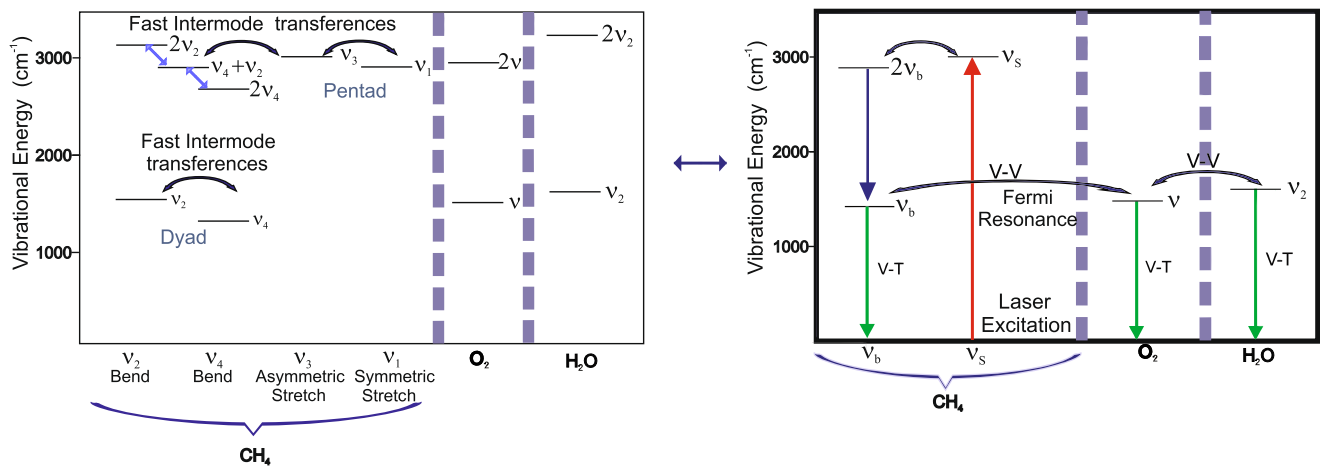
Fig. 1 The 11 excited level system is simplified to five. The figure does not show the nitrogen levels because they are not involved in the V–V energy exchanges

6. The first-order perturbation theory of the harmonic oscillator predicts a scale factor that relates the relaxation rates of high vibrational levels with the first excited state.
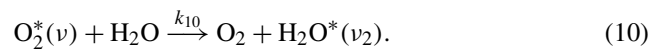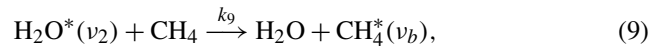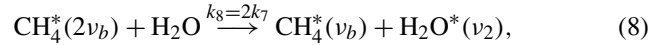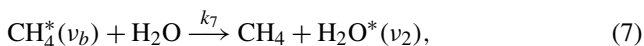
2.2 Processes involved in the model

After excitation of a methane molecule, the intermode transfer process redistributes the absorbed energy through collisions. The optically excited level ν_S transfers its energy at a fast rate to $2\nu_b$. This exchange can occur through collisions with species M (methane, nitrogen, oxygen or water) in its ground state and is described as
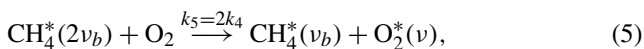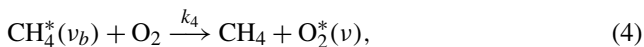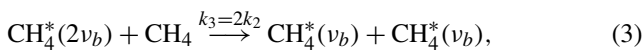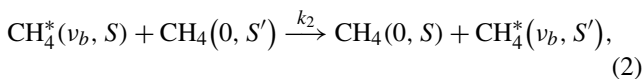
$$CH_4^*(\nu_S) + M \xrightarrow{k_1^M} CH_4^*(2\nu_b) + M. \tag{1}$$
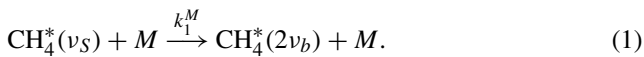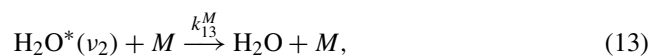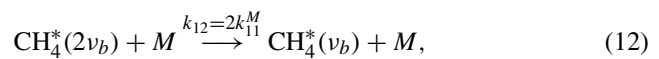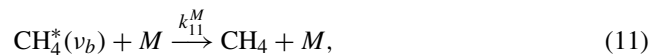
This process shows how the methane molecule releases a fraction of its internal energy $h(\nu_S - 2\nu_b)$ and becomes excited into the $2\nu_b$ state. The rate constant corresponds to k_r^M, where M represents the four possible molecules involved in the process and r is the process number.

The next processes involve the redistribution of energy between polyads and with oxygen and water, taking into account V–V transfers:

$$CH_4^*(\nu_b, S) + CH_4(0, S') \xrightarrow{k_2} CH_4(0, S) + CH_4^*(\nu_b, S'), \tag{2}$$

$$CH_4^*(2\nu_b) + CH_4 \xrightarrow{k_3=2k_2} CH_4^*(\nu_b) + CH_4^*(\nu_b), \tag{3}$$

$$CH_4^*(\nu_b) + O_2 \xrightarrow{k_4} CH_4 + O_2^*(\nu), \tag{4}$$

$$CH_4^*(2\nu_b) + O_2 \xrightarrow{k_5=2k_4} CH_4^*(\nu_b) + O_2^*(\nu), \tag{5}$$

$$CH_4 + O_2^*(\nu) \xrightarrow{k_6} CH_4^*(\nu_b) + O_2, \tag{6}$$

$$CH_4^*(\nu_b) + H_2O \xrightarrow{k_7} CH_4 + H_2O^*(\nu_2), \tag{7}$$

$$CH_4^*(2\nu_b) + H_2O \xrightarrow{k_8=2k_7} CH_4^*(\nu_b) + H_2O^*(\nu_2), \tag{8}$$

$$H_2O^*(\nu_2) + CH_4 \xrightarrow{k_9} H_2O + CH_4^*(\nu_b), \tag{9}$$

$$O_2^*(\nu) + H_2O \xrightarrow{k_{10}} O_2 + H_2O^*(\nu_2). \tag{10}$$
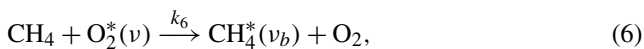
In process (2), S and S' represent two different symmetries. In (3), (5) and (8) the perturbation theory scale factor is used. The V–T processes are

$$CH_4^*(\nu_b) + M \xrightarrow{k_{11}^M} CH_4 + M, \tag{11}$$

$$CH_4^*(2\nu_b) + M \xrightarrow{k_{12}=2k_{11}^M} CH_4^*(\nu_b) + M, \tag{12}$$

$$H_2O^*(\nu_2) + M \xrightarrow{k_{13}^M} H_2O + M, \tag{13}$$

$$O_2^*(\nu) + M \xrightarrow{k_{14}^M} O_2 + M. \tag{14}$$

Considering all these processes, a new energy level diagram is possible. Figure 1 shows the original system of 11 excited states and a reduced one of five levels. This new model leads to a rate-equation system of five linear differential equations in which the ν_S mode population includes an oscillatory excitation term. This system can be solved numerically to find the time evolution of the level populations.

The rate constants are shown in Table 1, including values given by different authors. As far as we know, there are methane–water interactions that have not been published, so we estimated some relaxation rate values taking into account the values of other similar known interactions. For example, since process (1) has a rate of around 10^8 s^{-1} atm^{-1} with O_2, N_2 and CH_4, we assume that $k_1^{H_2O}$ should be of the same order of magnitude. In addition, typical relaxation rate values for polyatomic molecules in low vibrational levels were assigned to other V–V relaxation rates like (7) and (9) and to

Table 1 Rate constants of processes involved in the kinetic model

	Rate constants (s^{-1} atm^{-1})
$k_1^{CH_4}$	2.13×10^8 [1]; 5.3×10^8 [2]; 1.1×10^9 [3]; 1.1×10^9 [4]
$k_1^{O_2}$	4.6×10^8 [14]; 8.7×10^8 [16]
$k_1^{N_2}$	4.6×10^8 [16]; 8.7×10^8 [15]
$k_1^{H_2O}$	$\sim 10^{8a}$
k_2	2.7×10^8 [4]; 2.28×10^8 [14]; 2.7×10^8 [15]; 2.4×10^8 [16]
k_4	2×10^7 [4]; 3.27×10^7 [16]
k_6	3×10^7 [4]; 3.3×10^6 [16]
k_7	$\sim 2 \times 10^{7a}$
k_9	$\sim 2 \times 10^{7a}$
k_{10}	1.3×10^6 [6]
$k_{11}^{CH_4}$	8×10^5 [4]; 7.6×10^5 [15]; 7.9×10^5 [16];
$k_{11}^{O_2}$	1.3×10^5 [4]; 1.4×10^5 [16]
$k_{11}^{N_2}$	8×10^4 [4]; 7.6×10^4 [15]
$k_{11}^{H_2O}$	$\sim 10^{5a}$
$k_{13}^{CH_4}$	$\sim 10^{6a}$
$k_{13}^{O_2}$	10^6 [17]
$k_{13}^{N_2}$	10^6 [17]
$k_{13}^{H_2O}$	1.2×10^9 [6]
$k_{14}^{CH_4}$	1×10^6 [4]
$k_{14}^{O_2}$	6.3×10 [4]; 6.6×10 [6]
$k_{14}^{N_2}$	4×10 [4]
$k_{11}^{H_2O_2}$	1.1×10^6 [4]

[a]Typical V–V and V–T relaxation values for polyatomic molecules in low vibrational levels

Fig. 2 The *solid line* shows the model results with 0.04 % CH_4, 20 % O_2, 1 % H_2O and 78.96 % N_2 at atmospheric pressure. The *dashed line* corresponds to a sample of 0.04 % CH_4 and 99.96 % N_2 at atmospheric pressure. The model predicts a growth in the signal in the case of water presence. Both calculations were done considering a laser power of 176 mW, analogous to the experimental measurements. T is the laser modulation period (430 μs)
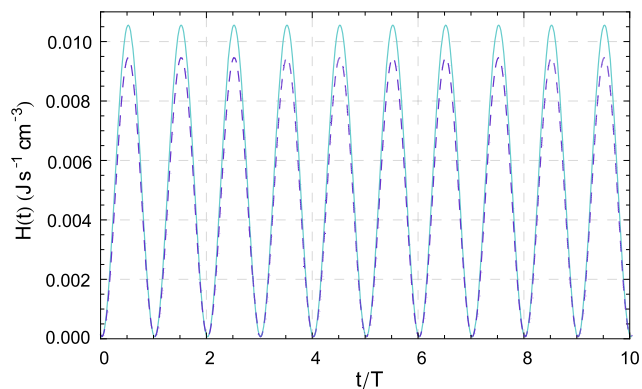
the V–T exchange described in (11). Having considered that we had approximate values of the different rates, we verified that the final numerical result does not change significantly even if these rates vary by one order of magnitude.

2.3 Results for the released power density

Once we have the solution for the populations, the next step calculates the released power density $H(t)$, defined as

$$H(t) = \sum_{r,M,L} h\nu_r k_r^M N_M N_L^*, \qquad (15)$$

where $h\nu_r$ is the energy involved in the V–T process r, N_M the population density of the fundamental state of the molecule M and N_L^* the population density of the excited molecule L. Using these results, in a previous paper [5] we confirmed that, exciting the sample at a modulation frequency of 2230 Hz, the presence of the typical percentage

(20 %) of oxygen in methane–air samples (3.95×10^{-4} atm of methane at atmospheric pressure) determines a 80 % reduction of the PA signal compared to the value obtained with pure N_2 as buffer. On the contrary, Fig. 2 shows that the heat generated by the modulated IR excitation in methane–nitrogen mixtures, calculated with our model, is comparable with that obtained in methane–air with 1 % of water. In this case, the energy stored in oxygen is released to kinetic energy through the interaction with water, and the amplitude shows a slightly higher value than in CH_4–N_2 mixtures. We show, in the next section, that this increase is also observed in the experimental results and is predicted by a kinetic model which includes all the methane and oxygen energy exchanges with water described in Sect. 2.2 [4, 7].

3 Photoacoustic cell

The cylindrical resonator with buffers at both ends is a widely employed PA cell. Excited at the resonance of the first longitudinal mode, it shows a low quality factor (less than 50 in most cases [1]). On the other hand, the cylinder, and also the sphere, excited at frequencies of the radial modes show a large quality factor (more than 1000 in some cases) but the microphone's location and the cell volume are critical for a good sensitivity [18, 19]. Generally speaking, in order to minimize the background signal due to window heating and multiple reflections, it is convenient to place the Brewster windows at the nodes of the acoustic mode. This configuration is not easily modelled and the design may be complicated [20]. As an example, we refer to the resonator designed by Meyer and Sigrist [21] that consists of a cylinder asymmetrically connected with two buffer volumes closed by windows at the Brewster angle. This cell

a Valve

b
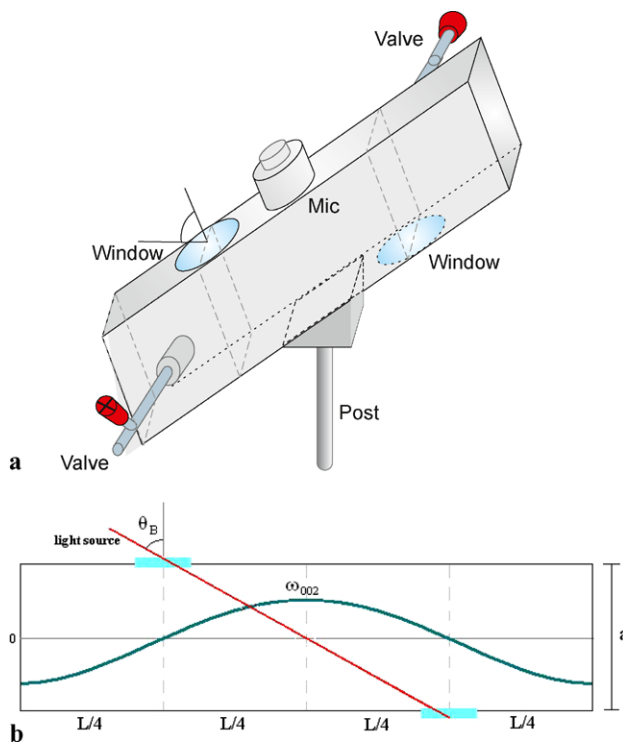
Fig. 3 (**a**) Scheme of the photoacoustic cell. (**b**) Side view of the photoacoustic cell. Notice the overlap between the acoustic mode ω_{002} and the laser path through the cell (θ_B: Brewster angle)

Fig. 4 Resonance curve. $\Delta f = 14$ Hz

was specially designed to excite a radial mode. Based on these requirements (high Q, small volume, windows placed at acoustic nodes), we designed an aluminum acoustic cavity shaped like a rectangular parallelepiped, shown in Fig. 3a. The length of the cell is $L = 15$ cm and the sizes of the transversal cross section are $a = 5$ cm and $b = 3$ cm. With these values, the eigenfrequencies can be calculated as
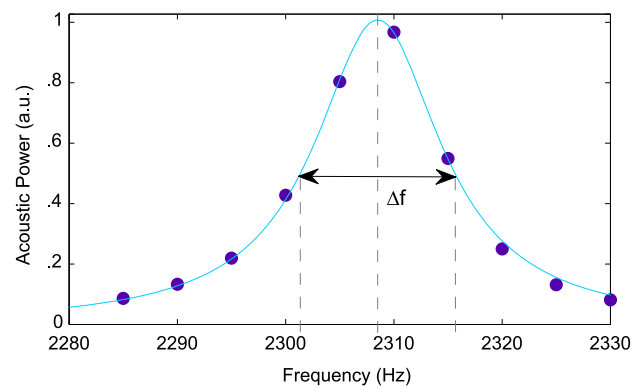
$$\omega_{lmn} = c_0\big((K_l)^2 + (K_m)^2 + (K_n)^2\big)^{1/2},$$

$$K_l = \frac{l\pi}{\alpha}, \qquad K_m = \frac{m\pi}{b}, \qquad K_n = \frac{n\pi}{L}, \qquad (16)$$

$$l, m, n = 0, 1, 2, \ldots,$$

where c_0 is the sound velocity and l, m and n are integers. The cell's dimensions ($a, b < L$) avoid the overlapping of resonance peaks and allow resolving neighbouring eigenfrequencies. In this way, we chose a modulation frequency of 2270 Hz, corresponding to the (002) mode with $\omega_{002} = c_0 2\pi/L$. Notice that the transverse modes are outside the microphone bandwidth (<10 kHz) and the odd longitudinal modes have a node at the microphone location. Finally, as the signal goes as $1/\omega$, the higher even longitudinal modes ((004), (006), ...) show lower amplitude.

The designed stand allows easy alignment of the cell in the beam path and great reproducibility (Fig. 3b). The CaF$_2$

windows are located at opposite sides at the acoustic nodes, at Brewster angles relative to the laser beam path.

The gas inlet and outlet ports were also placed at the (002) mode nodes to reduce possible perturbations due to flow turbulence. In addition, to attain lower losses, the cell's inner wall was mirror polished. The measured quality factor was 165 ± 1 (see Fig. 4), a higher figure than that of the cylindrical cells we used before, with similar resonant frequency. With all these features we obtained a low-noise cell with good sensitivity and high signal-to-noise ratio.

The eigenmodes $u_{lmn}(x, y, z)$ of this cell are of the form

$$u_{lmn}(x, y, z) = \cos(K_l x)\cos(K_m y)\cos(K_n z) \qquad (17)$$

and form a basis to expand any pressure distribution $p(x, y, z)$ as

$$p(x, y, z) = \sum_l \sum_m \sum_n A_{lmn}\cos(K_l x)\cos(K_m y)\cos(K_n z).$$

$$(18)$$

Here A_{lmn} is the pressure amplitude of the (lmn) mode and can be determined by solving the inhomogeneous wave equation with a released power density term. In Ref. [5], we showed that $H(t)$ can be expressed by a sum of a constant term representing the heat mean value and an oscillatory term multiplied by an amplitude H. As a result, the amplitude A_{002} turns out to be proportional to H and the normalized overlap integral (F_{002}).

Finally, the PA signal is proportional to H and the cell constant, which was determined by calibrating the system with a mixture of methane in nitrogen and using the absorption cross section of methane integrated over the OPO line width.

4 Experiment

The experiment was carried out using an OPO (M-Squared, model Firefly-IR-100, line width <10 nm, 190 mW at

3.3 µm), tuned at 3.3 µm, mechanically modulated with a chopper (Terahertz Tech. Inc. C-995) at the PA cell resonance frequency of 2270 Hz. The PA signal was acquired by a small, low-noise microphone (Knowles EK-3132) placed at the middle of one of the side walls (see Fig. 3a). A lock-in amplifier (Stanford Research SR830), which uses the chopper output as the reference signal, performed synchronous detection. A power meter (Gentec XLP12-15-H2) was used to measure the OPO power for normalization purposes. The measuring system (including the OPO wavelength, chopper repetition rate and communication with the lock-in amplifier) was automated and controlled by a computer.

The amplitude of the PA signal for different mixtures of methane (Alphagaz 99 %), air (L'Air Liquide 99.5 %, 80 % N_2, 20 % O_2, $H_2O <$ 5 ppmV, hydrocarbons < 1 ppmV, $CO + CO_2 <$ 0.5 ppmV) and water (distilled water at vapour pressure) was studied at 3.3 µm in order to compare experiment with theory. The gas mixtures were prepared in a line connected to a high-vacuum pump. The gas samples were prepared in the PA cell by mixing a fixed quantity of methane (3.95×10^{-4} atm), different pressures of water (from 0 to 0.016 atm or 1.6 %) and chromatographic air up to atmospheric pressure. Special care is needed when dealing with water measurements because of its fast adsorption at the cell walls. Heating the cell avoids this problem but most microphones do not withstand high temperatures. For this reason, we designed an alternative method. With a manometer (MKS Baratron model 622A) we determined the water pressure change inside the cell (without air) and noticed that, during the first minutes, it shows an exponential decay as a function of time but, later on, it changes linearly with a small slope. We found that at low water content, the pressure decays until it reaches a stationary value. At higher water amounts (more than 0.007 atm), after 10 min of adding water to the cell, the decay becomes linear and the rate can be obtained experimentally using the slope of a linear fit on the last part of the water pressure vs time curve. In this way, the amount of water inside the cell can be estimated within a 10 % error. After preparing the desired water quantity, the other gases (methane and air) were added to carry out the PA measurement.

Figure 5a shows the experimental results superimposed on the kinetic model prediction. In agreement with the model, it is clear that for 3.95×10^{-4} atm of methane and more than 0.6 % of water the signal is slightly greater than the one with methane and nitrogen only. It is important to point out that water has an absorption peak near the one of methane, at 3.3 µm. For this reason, it was necessary to obtain a calibration curve for water at that wavelength, so every measurement of the PA signal could be processed by subtracting the corresponding water signal taking into account amplitude and phase. Figure 5a shows the experimental results of the PA signal at different water contents superimposed on the values (solid line) calculated from the kinetic

a

b
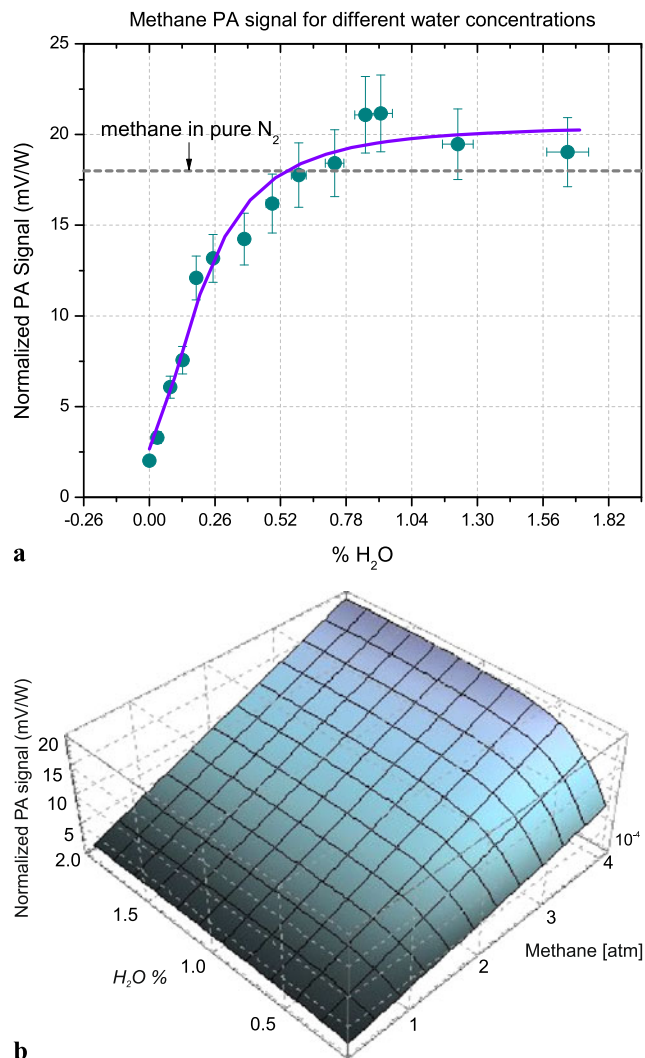
Fig. 5 (**a**) PA signal of methane at fixed pressure (3.95×10^{-4} atm) varying the water concentration. The water signal was subtracted from all the data. The *large error bars* in the last part of the curve are given by the 10 % of error in determination of water concentration in the sample. The *solid line* corresponds to the kinetic model (note that this curve is not a fit). (**b**) Kinetic model for PA signal varying both methane and water percentages in the mixture

model, based on the cell constant that had been determined from methane–nitrogen mixtures. No fitting parameter was used to compute the theoretical curve.

We calculated the PA signal for different concentrations of water and methane (Fig. 5b) taking into account that the ambient methane abundance is 1.7 ppmV. From the figure, it is clear that more than 0.7 % of water is high enough to recover the amplitude of the PA signal characteristic of methane–nitrogen.

Our system presented a limit of detection of 0.95 ppmV (with 0.7 % of water in 1 atm total pressure) given by the standard deviation of the background. A lower detection limit, adequate for ambient air monitoring, could be reached with a narrower line width OPO, since in our case

the methane integrated cross section is about one-tenth the maximum at 3.314 μm.

5 Conclusions

The new cell geometry shows advantages that allow fulfilling most of the usual PA requirements with a simple design. In this sense, it was possible to place the Brewster angle windows at the nodes of the acoustic mode, reducing significantly the background noise. As an extra benefit, we obtained a Q factor higher than the value of a cylindrical cell with $\lambda/4$ filters.

Water, a natural constituent of the atmosphere, proved to be an efficient collisional partner of oxygen. We found a good agreement between a simplified kinetic model and the measurements. It is important to remark that the knowledge of the setup constant together with this model allows predicting quantitatively the PA signal from methane–air–water samples.

References

1. A. Miklós, P. Hess, Z. Bozóki, Rev. Sci. Instrum. **72**, 1937 (2001)
2. S. Bernegger, M.W. Sigrist, Infrared Phys. **30**, 375 (1990)
3. A. Miklós, C. Lim, W. Hsiang, G. Liang A.H. Kung, A. Schmohl, P. Hess, Appl. Opt. **41**, 2985 (2002)
4. S. Schilt, J.-P. Besson, L. Thévenaz, Appl. Phys. B **82**, 319 (2006)
5. N. Barreiro, A. Vallespi, G. Santiago, V. Slezak, A. Peuriot, Appl. Phys. B **104**, 983 (2011)
6. D.L. Huestis, J. Phys. Chem. A **110**, 6638 (2006)
7. A.A. Kosterev, Y.A. Bakhirkin, F.K. Tittel, S. Mcwhorter, B. Ashcroft, Appl. Phys. B **92**, 103 (2008)
8. A. Veres, Z. Bozóki, Á. Mohácsi, M. Szakáll, G. Szabó, Appl. Spectrosc. **57**, 900 (2003)
9. T. Laurila, H. Cattaneo, T. Pöyhönen, V. Koskinen, J. Kauppinen, R. Hernberg, Appl. Phys. B **83**, 285 (2006)
10. R. Lewicki, G. Wysocki, A.A. Kosterev, F.K. Tittel, Appl. Phys. B **87**, 157 (2007)
11. G. Wysocki, A.A. Kosterev, F.K. Tittel, Appl. Phys. B **85**, 301 (2006)
12. A.A. Kosterev, T.S. Mosely, F.K. Tittel, Appl. Phys. B **85**, 295 (2006)
13. M. López-Puertas, G. Zaragoza, B.J. Kerridge, F.W. Taylor, J. Geophys. Res. **100**, 9131 (1995)
14. L. Doyennette, F. Menard-Bourcin, J. Menard, C. Boursier, C. Camy-Peyret, J. Phys. Chem. A **102**, 3849 (1998)
15. C. Boursier, J. Ménard, L. Doyennette, F. Menard-Bourcin, J. Phys. Chem. A **107**, 5280 (2003)
16. C. Boursier, J. Ménard, L. Doyennette, F. Menard-Bourcin, J. Phys. Chem. A **111**, 7022 (2007)
17. H.E. Bass, R.G. Keeton, D. Williams, J. Acoust. Soc. Am. **60**, 74 (1976)
18. A. Karbach, P. Hess, J. Appl. Phys. **58**, 3851 (1985)
19. S. Schilt, L. Thévenaz, M. Niklès, L. Emmenegger, C. Hüglin, Spectrochim. Acta, Part A **60**, 3259 (2004)
20. S. Bernegger, M.W. Sigrist, Appl. Phys. B **44**, 125 (1987)
21. P.L. Meyer, M.W. Sigrist, Rev. Sci. Instrum. **61**, 1779 (1990)